Direct Contact Electroplating Sequence Without Initial Seed Layer for Bifacial TOPCon Solar Cell Metallization

Benjamin Grübel, Gisela Cimiotti, Christian Schmiga, Varun Arya, Bernd Steinhauser, Norbert Bay, Michael Passig, Damian Brunner, Markus Glatthaar, and Sven Kluska

***Abstract*—The metallization of bifacial tunneling oxide and passivating contacts (TOPCon) solar cells without initial metal seed layer by electroplating of Ni/Cu/Ag is demonstrated. The presented approach allows a lead-free metallization with narrow contact geometries and low contact resistivity. A metal plate provides electrical contact to the silicon via micrometer size laser contact openings and allows electroplating of bifacial TOPCon solar cells using industrial type inline plating tools without the need of a previously applied seed layer. Challenges such as direct contacting of silicon and dissolution of contacts are identified, and potential solutions are discussed. An optimized process sequence is developed and with this approach a solar cell efficiency of 22.5% is demonstrated on industrial bifacial TOPCon solar cells reaching the same level as the screen-printed reference solar cells.**

***Index Terms*—Forward bias plating (FBP), light induced plating (LIP), passivating contacts, silicon solar cells, tunneling oxide and passivating contacts (TOPCon).**

I. Introduction

SOLAR cells featuring carrier selective contacts such as tunneling oxide and passivating contacts (TOPCon) consisting of a thin oxide layer and a highly doped poly-Si, which significantly reduces contact recombination have attracted an increased interest lately. Their potential was already shown on an *n*-type both sided contacts lab cell by Richter *et al.* [1] with 25.8% efficiency [2] and single-sided contacted IBC lab cell by Haase *et al.* [3] with 26.1% both on 4 cm² sample size. The industrial implementation referred as i-TOPCon featuring a boron emitter passivated by AlO_x/SiN_x on the front side and TOPCon/SiN_x on the rear side is seen as next technology after passivated emitter and rear cell (PERC).

A common challenge in industrial mass production is upscaling of the processes. Metallization is a key aspect in the production of bifacial TOPCon solar cells. In order to guarantee the functionality of the passivating contact any damage of the TOPCon layer must be avoided. For screen-printed metallization most of recent publications require a thickness of at least 100 nm of the TOPCon layer to ensure its functionality [4]–[6]. For UV (355 nm) picosecond (ps)-laser ablation before plating the contacts 60–70 nm are sufficient so that the tunneling oxide remains intact as the penetration depth of the laser is around 50–60 nm [3], [7]. Furthermore, contacting these laser contact openings via electroplating of Ni/Cu/Ag would allow an alternative lead-free metallization technique with narrow contact geometries ($\leq$ 25 μm), low contact resistivity ρ_c ($<$ 1 mΩcm²) [8] with high throughputs and low cost of ownership (COO) showed by Kluska *et al.* [9].

Plating of bifacial PERT solar cells by simultaneous batch deposition on n and p-side using electroless Ni plating finished by Ag capping layer as demonstrated by Tous *et al.* [10] might be suitable for bifacial TOPCon solar cells. This method requires a silicon selective surface activation of the silicon interface. Simultaneous bifacial electroplating requires a sufficient lateral conductivity of a seed layer along the wafer surface [11], [12]. In this article, we present a new plating process sequence for bifacial TOPCon solar cells omitting the necessity of a conductive seed layer by contacting directly the silicon within laser contact openings. This approach was introduced by Gensowski *et al.* [13] as direct contact plating. It enables successive single-sided electroplating on each side of a bifacial solar cell. State-of-the-art single sided plating tools such as inline plating tools were used in this work to demonstrate direct contact plating for bifacial TOPCon solar cells.

II. Experimental

A. Approach and Plating Conditions

The direct contact plating process sequence is displayed in Fig. 1. Prior to the plating process, the dielectric antireflection coating on both sides of the solar cell is locally removed by laser ablation using a UV ps-laser corresponding to the desired grid

Manuscript received September 21, 2020; revised December 3, 2020; accepted January 8, 2021. Date of publication February 11, 2021; date of current version April 21, 2021. This work was supported in part by the German Federal Ministry for Economic Affairs and Energy within the Projects "GENESIS" under Grant 0324274VC and "TALER" under Grant 03EE1021B. *(Corresponding author: Benjamin Grübel.)*

Benjamin Grübel, Gisela Cimiotti, Christian Schmiga, Varun Arya, Bernd Steinhauser, Markus Glatthaar, and Sven Kluska are with the Fraunhofer Institute for Solar Energy Systems, 79110 Freiburg, Germany (e-mail: benjamin.gruebel@ise.fraunhofer.de; gisela.cimiotti@ise.fraunhofer.de; christian.schmiga@ise.fraunhofer.de; varun.arya@ise.fraunhofer.de; bernd.steinhauser@ise.fraunhofer.de; markus.glatthaar@ise.fraunhofer.de; sven.kluska@ise.fraunhofer.de).

Norbert Bay, Michael Passig, and Damian Brunner are with the RENA Technologies GmbH, 79108 Freiburg, Germany (e-mail: norbert.bay@rena.com; michael.passig@rena.com; damian.brunner@rena.com).

Color versions of one or more figures in this article are available at https://doi.org/10.1109/JPHOTOV.2021.3051636.

Digital Object Identifier 10.1109/JPHOTOV.2021.3051636

This work is licensed under a Creative Commons Attribution 4.0 License. For more information, see https://creativecommons.org/licenses/by/4.0/

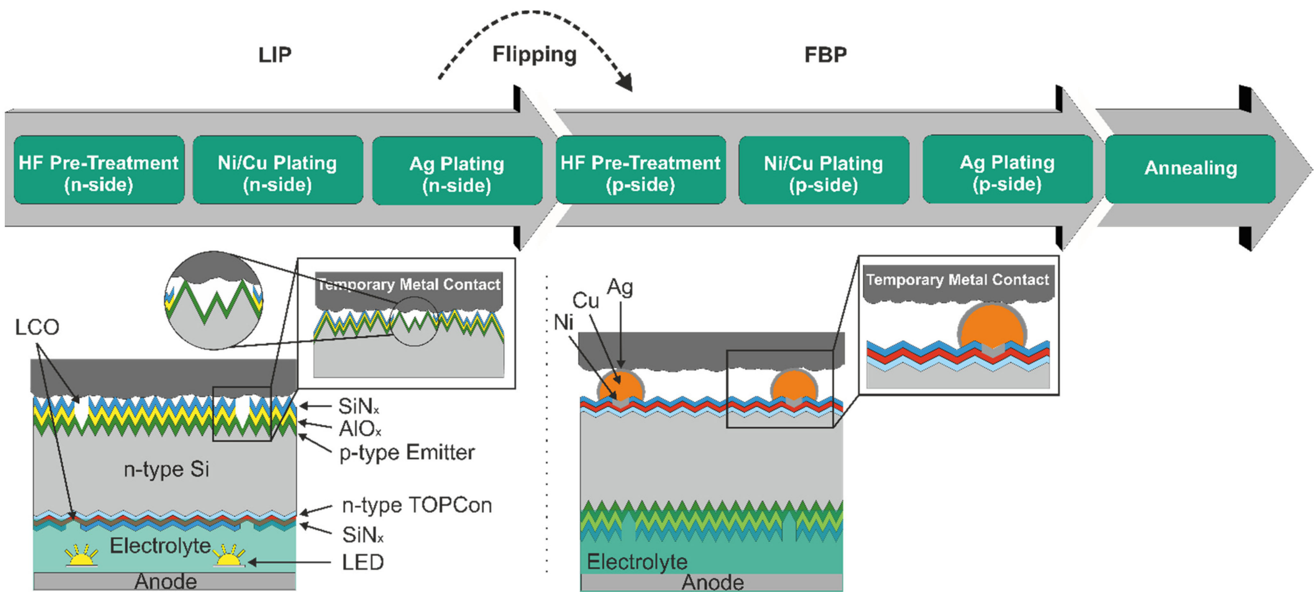

Fig. 1. Direct contact electroplating sequence including HF pretreatment and Ni/Cu/Ag plating with an optional annealing for bifacial TOPCon solar cells. The mentioned side refers to the side where the deposition takes place. The contacting of the solar cell is performed by a temporary metal contact consisting of a metal plate placed on surface of the solar cell. The side contacting the laser contact openings is coated with a Ni layer.

design. According to the intended orientation of the solar cell toward the sun, the *n*-type doped side is defined as rear side, whereas the *p*-type doped side is referred to as front side in this work. The process sequence for plating on the rear side consists of a single-sided low concentrated HF pretreatment in order to remove any oxide layer within the laser contact opening (LCO). Subsequently, Ni and Cu plating is performed by light induced plating (LIP) by immersing the laser patterned solar cell precursor single-sided in the plating electrolyte while being illuminated by LEDs positioned in the electrolyte. On the nonimmersed (dry) side of the wafer the LCOs are temporarily contacted by a metal plate as visible in Fig. 1(zoomed circle) with a constant current and a voltage limit of 20 V. The metal plate features a Ni coating on the side facing the solar cell. For this plate a small margin (∼1 cm) on each side is kept to avoid wetting of the temporary metal contact by the electrolyte, which would lead to preferential deposition onto the metal plate instead of the solar cell. In order to improve the contacting, the temporary metal contact can be pressed onto the wafer. The plated metal stack is finished with a single-side chemical Ag capping carried out by electroless (immersion) plating. Subsequently, the solar cell is flipped and almost the same process sequence for depositing Ni and Cu is applied. However, this time the temporary metal contact is contacting the already plated grid on the rear side and no light is required for plating as the pn-junction is under forward bias (forward bias plating (FBP) [14]). The front side is capped in the electroless Ag bath as well. The selected electrolytes for Ni, Cu, and Ag plating are presented in Table I. All plating processes are performed in lab-type versions of the inline plating tool "InCellPlate" of the company Rena Technologies GmbH. All plating steps are single-side processes apart from the annealing step. The light intensity of the LEDs of the inline tools can be adjusted so that the current generated by the solar cells can be controlled. This means that for an external current that is lower/higher than the generated current of the solar cell, the external / solar cell current is limiting the accessible current for the plating deposition. In this work, the light intensity was kept constant at a level so that the current generated by the solar cell is higher than the external current. The plated solar cells were annealed after plating in order to reduce the contact resistance and increase the contact adhesion [15], e.g., by an offline laser based rapid thermal processing oven [16].

TABLE I
PLATING PARAMETERS, ELECTROLYTES, AND RESULTING LAYER THICKNESSES USED IN THIS WORK TO PLATE A STACK OF NI/CU/AG ON BORON EMITTER (FRONT SIDE) AND TOPCON (REAR SIDE) SURFACE

Name		Helios Nickel EP610	Helios Copper EP2	Helios Silver IM452
Supplier			MacDermid	
Temperature	°C	50	25	50
Plating Current Density	A/dm²	2	4-9	Electroless
Plating Time	s	180	300	60
Layer Thickness Front Side / Rear Side	µm	1 / 1	4-6 / 8-10	0.5 /0.5
Deposited Mass Front Side / Rear Side	mg	3-5 / 3-5	30-35 / 40-45	1-2 / 1-2

The contacting of the solar cell to perform the electroplating process is an essential aspect for the presented process sequence. Especially, the homogeneous contacting of a textured silicon surface is challenging as outlined in the sketch in Fig. 1(zoomed circle). As the contacted area is unknown a precise contact resistance is not accessible. However, a way of characterizing

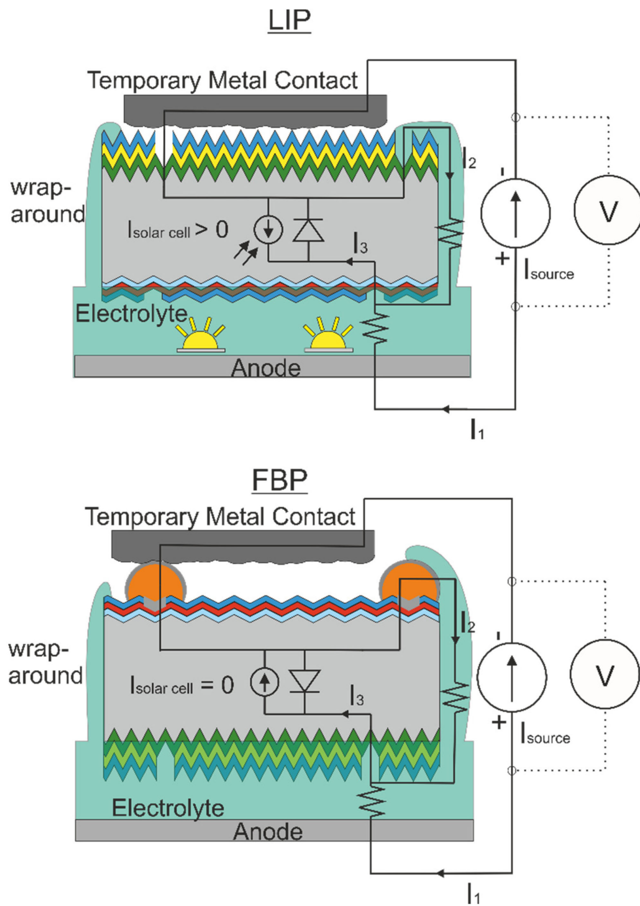

Fig. 2. Simplified equivalent circuit diagram for LIP and FBP with two meshes each. For LIP in the outer mesh, the current path I_{source} $(= I_1)$ includes the current source contacting the anode, followed by the electrolyte being in contact with the rear side of the solar cell. The front side of the solar cell is in contact with the temporary metal contact, which is directly contacted by the negative port of the current source. During LIP the solar cell generates a photocurrent $I_{\text{solar cell}}$. The voltage drop is measured over the current source, therefore including all components. The voltage depicts the required voltage to distribute the source current. For the case of a wrap-around of the electrolyte onto the nonimmersed side, the inner mesh describes a current path I_2 connecting front and rear side via the electrolyte, which will be covered in Section III.C. The current I_3 is the current through the solar cell towards the rear side combining I_1 and I_2. For FBP a similar equivalent circuit can be used with just the solar cell flipped such as it behaves essentially like a diode. It must be mentioned that the sketch is only used for clarification of all components included for the voltage determination omitting nonlinear effects such as diode behavior of the cell and capacitive components. For a precise equivalent circuit the author would like to refer to Lennon *et al.* [17].

the quality of this contact is to measure the voltage required for driving a predefined current in a galvanostatic plating process. This voltage is influenced by several aspects of the plating process apart from the contacting, as will be shown below. In Fig. 2, equivalent circuit diagrams with two constellations of the solar cell during LIP or FBP on the rear and front side, respectively, are introduced. For LIP in the outer mesh (I_1) the current passes the anode, toward the rear side (n) of the solar cell via the electrolyte. The front side of the solar cell is connected with the temporary metal contact, which is in contact with the current source. As during the plating process a wrap-around of the electrolyte is observed onto the nonimmersed side (front side), a second inner mesh is introduced. The inner mesh represents the current path connecting the front and rear side of the solar cell directly via the electrolyte. This behavior can influence the deposition process, as will be shown below in Section III.C. During LIP the photocurrent generated by the solar cell is typically larger than the source current ($I_{\text{source}} < I_{\text{solar cell}}$). The voltage is measured over the current source and characterizes the voltage needed to drive the source current. Typical voltages measured for PERC plating are below 3 V. For FBP a similar equivalent circuit is used, only the solar cell is flipped acting essentially as diode.

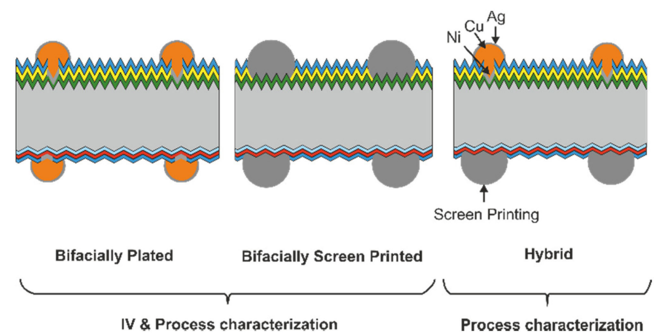

Fig. 3. TOPCon solar cell layouts used in this work including a bifacial plated (left) or bifacial screen-printed design (middle) and a hybrid design (right) with plated contacts on the front side and screen-printing on the rear side.

B. Solar Cells

In this work, industrial bifacial *n*-type TOPCon solar cell precursors (158.75 × 158.75 mm²) after passivation and optimized for screen-printing metallization were selected as shown in Fig. 1. The textured front side consists of a *p*-type boron emitter passivated by an AlO_x/SiN_x stack. The rear side features an *n*-type TOPCon layer exceeding 100 nm coated with SiN_x. Three metallization designs were selected as displayed in Fig. 3. On both sides of the bifacial plated solar cells laser patterning with 9 busbars and 96 fingers were performed with an UV ps-laser followed by a firing in an industrial conveyer belt furnace. The precursors were then plated on both sides according to the plating sequence presented in Section (II. A). Screen printed cells were used as reference with identical grid design. The IV measurements were performed at a flash IV tester (cetisPV-Celltest3 / HALM). A Grid$^{\text{Touch}}$ contacting [18] unit was used due to a limitation of the maximum number of contacting rails in the IV tester. In addition, hybrid TOPCon solar cells were produced with screen-printed contacts on the rear side and plated contacts of the front side. This design was only used to characterize the plating results and effects.

The dimensions of the metal contacts were characterized by a confocal laser microscope (LEXT OLS4000). More than 50 positions randomly distributed over the cell were measured on each side of the processed solar cells to get the general appearance of the fingers as well as the contact dimensions (height and width). For more extensive characterization of the contact properties some additional samples were processed with the opposite process sequence as displayed in Fig. 1 by plating the front side first followed by the rear side. Contact resistivity

TABLE II
IV VALUES OF THE BEST BIFACIAL PLATED AND REFERENCE (SCREEN-PRINTED) TOPCON SOLAR CELLS MEASURED

Metallization	Voc (mV)	Jsc (mA/cm²)	FF (%)	pFF (%)	η (%)	Rs (Ωcm²)
Plating	686	40.1	81.9	83.2	22.5	0.4
Reference	690	39.9	81.9	83.3	22.5	0.4

measurement of the plated contacts via transfer length method (TLM) [19] were performed as well as contact angle measurements on each side of the solar cell samples on an OCA 20 contact angle system (Dataphysics).

III. Results and Discussion

A. IV Results

In Table II, the IV results of the solar cells are presented. The reference solar cells (bifacial Ag/AgAl screen printed TOPCon solar cells) of the same precursor batch achieved an efficiency of $\eta = 22.5\%$. With the presented direct contact plating sequence an identical efficiency of $\eta = 22.5\%$ was reached. The pseudofill-factor *pFF* is similar for both metallization groups. The series resistance is identical for both solar cells resulting in a *FF* of 81.9%. The lower open-circuit voltage V_{oc} of the plated solar cell is compensated by a higher $J_{\rm sc}$ (+ 0.2 mA/cm²) originating mainly from smaller contact widths resulting in the end in an identical efficiency. The limited number of solar cells processed, does not allow a statistical evaluation. The $V_{\rm oc}$ of all samples is subject of sample to sample variation. It has to be noted that the grid design (finger and busbar number) was optimized for screen printed reference solar cells and not changed for the plated solar cells in order to simplify the comparison.

Additionally, the contact resistivity of the plated TOPCon solar cells was characterized by TLM measurements. The contact resistivity of plated Ni/Cu/Ag contacts on boron emitter and TOPCon surfaces was measured as $\rho_{\rm c,\ boron} = (0.3 \pm 0.2)$ mΩcm² and $\rho_{\rm c,\ TOPCon} = (0.4 \pm 0.4)$ mΩcm², respectively. The measured values are in the range of recently published contact resistivities [8]. The measured finger resistivity for the plated contacts is around $(1.79 \pm 0.2) \times 10^{-8}$ Ω·m only slightly higher than the literature value for Cu (1.72×10^{-8} Ω·m) [20].

B. Direct Contact Plating

In Fig. 4 exemplary and representative images of deposited fingers are displayed depending on the contacted surface during the plating process. Hereby the plating process of Fig. 1 was used as well as the opposite order by plating the *p*-type doped side first in order to characterize potential differences of the sequence order. Additionally, in Table III and Fig. 5 the average finger width and height are displayed for each case in combination with a distribution of finger width and height along one finger on the rear side of a solar cell. The ablation width of the laser process for both sides is in the range 14–16 μm. It has to be taken into account that plated fingers are influenced by the

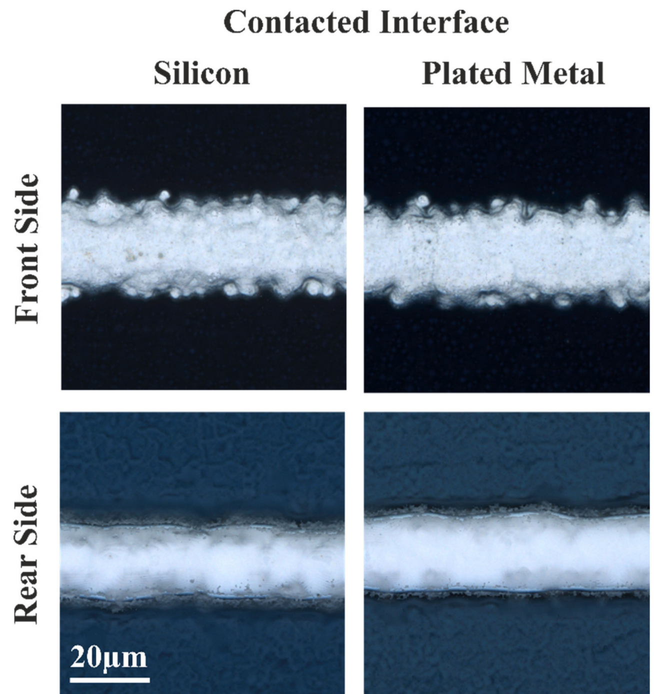

Fig. 4. Laser microscopy images of plated fingers on front and rear side of a TOPCon solar cell in dependency of the contacted interface.

TABLE III
CHARACTERIZATION OF THE FINGER DIMENSIONS ON FRONT AND REAR SIDE OF A TOPCON SOLAR CELL IN DEPENDENCY OF THE CONTACTED INTERFACE

	Contacted Interface			
	Silicon		Plated Metal	
	Width (µm)	Height (µm)	Width (µm)	Height (µm)
Front side	21.1 ± 0.7	4.6 ± 0.4	24.9 ± 2.1	4.3 ± 0.6
Rear Side	23.1 ± 0.7	9.3 ± 0.3	23.1 ± 1.6	8.9 ± 1.8

plating tool design, which may lead to inhomogeneities in terms of width and height over the wafer area. These are shown to be nonsignificant in terms of maximum IV performance and solar cell efficiency [21]. Apart from this phenomenon no local inhomogeneities or dendritic finger growth were visible. The differences in appearances from the fingers on front and rear side in Table III supposedly originate from different surfaces topography and finger heights limiting the leveling effect of the electrolyte. Independently of the sequence order the plated contacts have a similar appearance.

In Table IV, the measured voltage (see Fig. 2) during plating for different contacted interfaces is shown depending on the plating current density. The voltage is a sum of several contributions such as the contacting, the solar cell and the parts inside the electrolyte. If silicon within the LCO is the contacted interface during plating, a voltage exceeding 20 V is required to distribute the current density of 2 A/dm² for Ni plating. As

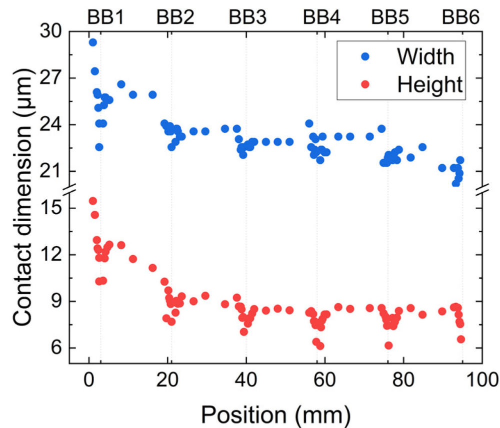

Fig. 5. Exemplary width and height distribution along one finger on the rear side of a TOPCon solar cell. The finger has higher dimensions at the edge of the wafer and lower values at the intersections with the busbars. The dimensions from BB1 to BB9 are symmetrical with respect to BB5. For a deeper understanding of this effect, the author would like to refer to Merhi *et al.* [21].

TABLE IV
MEASURED PLATING VOLTAGE ACCORDING TO FIG. 2 FOR A DISTRIBUTED PLATING CURRENT DENSITY FOR THE DIFFERENT CONTACT INTERFACES BY THE TEMPORARY METAL CONTACT (LCO/PLATING) FOR LIP AND FBP.

Plating	Contacted Interface	Temporary Metal Contact Pressure (N/cm²)	Plating Current Density (A/dm²)	Plating Voltage (V)
LIP	Silicon	6.8×10^{-3}	2(Ni) 8 (Cu)	> 20 (Ni and Cu)
	Silicon	122.6×10^{-3}	2(Ni) 8 (Cu)	< 5 (Ni) 10-15 (Cu)
FBP	Plated Metal	6.8×10^{-3}	2(Ni) 8 (Cu)	< 5 (Ni and Cu)

Optionally, weights were put onto the temporary metal contact to increase the contact pressure between the temporary metal contact and the solar cell.

this is abovementioned the adjusted voltage limit the target current density could not be reached. To improve the contacting of the interface between the temporary metal contact and the LCO, the temporary metal contact was gently pressed onto the wafer with a contact pressure of 122.6×10^{-3} N/cm². This led to a reduction of the required plating voltage for Ni (<5 V at 2 A/dm²) and Cu (10–15 V at 8 A/dm²) independently of which side of the TOPCon solar cells was plated first. As only the contact interface between the temporary metal contact and the LCO is modified the lowering of the plating voltage can be fully attributed to the improved contacting. Presumably the increased pressure increases the actual contact area to the textured silicon, as more pyramid tips come into contact with the applied metal plate as well as the contact area for every single pyramid is increased. The applied pressure was moderately small so that the wafer did not suffer any structural impact. According to the IV results and additional microscopy characterization of the surface after applying such a pressure no impact was observed. As a metal contact is applied onto the wafer, in an industrial approach it is thinkable that the contact pressure can be either generated by the weight of the metal contact itself or by adjustable springs applying pressure onto the metal contact. When flipped, the contacted interface countering the temporary metal plate consists of a plated Ni/Cu/Ag metal stack. Therefore, without the need of additional pressure, a plating voltage around 5 V was measured as the first Ni deposition takes place followed by a drop in voltage within seconds fluctuating around 2–3 V even for Cu plating where higher current densities (8 A/dm²) were used.

Plating of bifacial TOPCon solar cells requires higher plating voltages for contacting the silicon within the LCO. Nevertheless, inhomogeneity of the plated contacts due to inhomogeneous contacting could not be observed. The high voltage was found to originate mainly from the limited contacted area of the temporary metal contact. However, due to the limited contact area the high voltage might lead to side effects such as damage on the silicon surface due to small discharges (corona discharge [22]). Even though the contact pressure between the temporary metal contact and the LCO significantly reduced the plating voltage for Ni plating, Cu plating with a plating current density of 8 A/dm² still required around 10–15 V. A further increase of deposition rate and the plating current density for higher throughputs would lead to an increase in the required plating voltage. Although the homogeneity is not affected smaller contact cross sections (height and width) can be a consequence as the full plating current is not reached.

C. *Contact Modifications due to Electrolyte Wrap-Around*

The presented plating sequence for bifacial TOPCon solar cells consists of plating the full Ni/Cu/Ag stack on one side of a solar cell followed by plating of the same metal stack on the opposite side. During the plating process–independently of which side is plated–a wrap-around of the electrolyte occurs, wetting the surface in a range of 5 mm wide area on the otherwise dry side close to the edge. The wetting results in an additional current path as displayed in Fig. 2 by the inner mesh (I_2). The origin of the edge wetting is most likely due to wetting properties along the rough wafer surface (texture/polished texture surface). Furthermore, contact angle measurements support that the general wettability properties of the dry surface play a major role. Moderate hydrophobic surfaces prevent electrolyte wrap around, which was usually experienced at Fraunhofer ISE for single-side plating of PERC solar cells with measured contact angles above 40°. The TOPCon solar cells plated in this work showed a more hydrophilic surface behavior with contact angles in the range of 10°–20° at the wafer edge on the rear side whereas in the middle of the cell no contact angle was measurable. On the front side the wetting with a droplet is spreading instantly on the whole surface, confirming the observation that the wrap around occurs faster on the front side than on the rear side. Although, PERC and TOPCon solar cells feature both SiN_x surfaces, the difference in terms of wettability is evident, but yet unclear and part of ongoing research.

If a both side metallized solar cell is fully immersed into an electrolyte and illuminated a plating process occurs with a deposition on the *n*-type doped side whereas an oxidation

TABLE V
DEFINITION OF THE CURRENT PATHS $I_{1\text{-}3}$ FOR THE RELATION BETWEEN SOURCE CURRENT I_{SOURCE} AND CURRENT OF THE SOLAR CELL $I_{\mathrm{SOLAR\ CELL}}$ FOR LIP AND FBP.

	Intended Deposition	$I_{\mathrm{source}} < I_{\mathrm{solar\ cell}}$	$I_{\mathrm{source}} > I_{\mathrm{solar\ cell}}$
LIP	Rear side	$I_1 = I_{\mathrm{source}}$ $I_2 = I_{\mathrm{solar\ cell}} - I_{\mathrm{source}} > 0$ $I_3 = I_{\mathrm{solar\ cell}}$ Deposition on rear Dissolution on front	-
FBP	Front side	-	$I_1 = I_{\mathrm{source}} = -I_2 + I_3$ $(I_2 < 0)$ Deposition on front and rear

Additionally, the intended deposition side and actual deposition or dissolution on each side is mentioned.

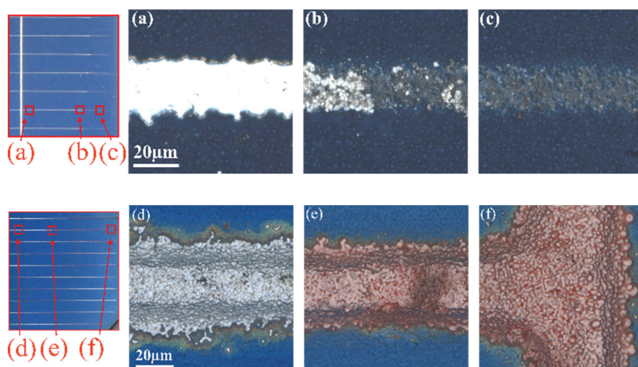

Fig. 6. Two cases (1,2) are displayed with zoomed scan images and laser microscopy images at specified positions at the edge of a wafer. Case (1) (a–c) describes LIP with the source current I_{source} smaller than the photo generated current of the solar cell $I_{\mathrm{solar\ cell}}$. In case (2) (d–f) FBP was performed in the dark meaning that the solar cells act essentially as a diode. For case (1) on image (c) the removal of the metal showing the LCO is displayed at the edge of the solar cell. For case (2) screen-printed contacts are shown, revealing a change of the contact color to an orange appearance indicating the deposition of Cu.

process, hereby dissolution of metal takes place on the *p*-type doped side. The resulting plating current I_2 equals the generated current by the solar cell [17], [23]. In this work two cases can be deduced during LIP (1) and FBP (2) by adding an additional source current I_1 (Fig. 2) as displayed in Table V.

For LIP, the external current source, which controls the deposition is smaller than the photo generated current by the solar cell and therefore limits the plating current. Due to the wrap-around, the surplus of generated electrons and holes by the solar cell can result in a reduction process on the rear side and an oxidation process in the wetted areas on the front side of the solar cell. If there are already metal contacts the front side the oxidation acts as dissolution of these contacts. In Fig. 6, this effect was characterized on plated solar cells. The magnified scan image for case (1) shows that the appearance of the fingers is changing toward the edge of the solar cell. Additional laser microscopy images were made along one finger. In image (a) the finger is shown close to the busbar with a similar appearance to a finger in the center of the solar cell (Fig. 4). Image (b) shows a change of appearance of the finger in such way that in image (c) finger close to the edge of the cell reveals a typical shape of a LCO pointing out the dissolution of the contacts at this position.

For LIP, $I_{\mathrm{source}} > I_{\mathrm{solar\ cell}}$ would also be feasible. However, the solar cell would be operated in reverse, making a voltage limitation necessary to avoid reverse voltage breakthrough of the solar cell making this process undesirable.

For FBP, as the solar cell is not illuminated, no additional electrons/holes are generated by the solar cell, so that only the source current (I_{source}) is used for the plating process resulting in an exclusive deposition in all wetted areas. In Fig. 6 case (2) the solar cell design Hybrid was used for clarification. The finger in a nonwetted area is typical for a screen-printed finger (d). In the wetted area the finger essentially changes its color appearance revealing the deposition of Cu (e–f). The same effect was also visible for a both side plated solar cell.

The effect of wrap-around of the electrolyte is occurring independently of which side is contacted. As both sides are plated anyway the wetting of both sides itself is not critical. However, if the photo generated current during LIP exceeds the source current, wetting of contacts on the *p*-type doped front side is detrimental as the contacts are dissolved during the plating process. If the *p*-type doped side is not metallized yet the LCO is oxidized, being negligible as this side will be treated with HF before the plating meaning that the *p*-type side should be plated last. If FBP is performed deposition on both sides occurs. At first sight deposition on both sides might be favorable to dissolution of contacts. However, for bifacial plating initially both sides are unmetallized. As the plating time of Cu is exceeding the Ni plating time, the wetted area is greater during Cu plating. Therefore, there is a risk of Cu deposition directly within the LCO, which should be avoided due to strong Cu diffusion into silicon [24] so that the *n*-type doped side should be plated at first. As long as the wrap around is not avoided, plating of the n-doped side first followed by the p-doped side is suggested, as displayed in Fig. 1, as no contact dissolution would occur on the *p*-type doped side and the additional deposition on the *n*-type doped side would only thicken the wetted contacts causing no harm.

IV. Conclusion

In this work, we successfully successively conducted electroplating by directly contacting silicon within local laser contact openings with a temporary metal contact. It has been shown that an inline plating process can be performed for bifacial TOPCon solar cells without the need of a conductive seed layer on at least on side in order to distribute the plating current into the solar cell. Electrical contacting especially of silicon was successfully conducted to perform the plating process but was also identified as challenging aspect for increasing current density predominantly used on an industrial dimension. An industrial implementation is not fully known yet but improving the contacting is part of further optimization. By pressing the temporary metal contact onto the solar cell, the contacting was significantly improved by reducing the plating voltage from > 20 V to 10–15 V for Cu plating allowing a homogeneous deposition of metal contacts.

Furthermore, contact dissolution was observed during the plating process due to wrap-around of the electrolyte. The origin of the electrolyte wrap-around was identified to be the highly hydrophilic nature of the both surfaces of the used TOPCon samples. A method has been introduced to understand the effects caused by the wrap-around of the electrolyte. The wrap-around causes dissolution in the wetted areas during LIP at high photocurrents on one hand and additional deposition during FBP in the wetted areas on the other hand. Plating of the *n*-type doped side first followed by *p*-type doped side allows to neglect the occurrence of the wrap-around with regard to the IV characteristics of the solar cell. Improving the contacting for the plating process as well as preventing the wrap-around of the electrolyte will be part of ongoing work. As a result, industrial TOPCon solar cell precursors were plated with the developed plating process sequence successively on both sides achieving an efficiency of $\eta = 22.5\%$ comparable to bifacial screen-printed reference TOPCon solar cells.

Acknowledgment

The authors would like to thank their colleagues at the Fraunhofer institute for solar energy systems (ISE) for their help with the experiments and solar cell characterization.

References

[1] A. Richter *et al.*, "*n*-Type Si solar cells with passivating electron contact: Identifying sources for efficiency limitations by wafer thickness and resistivity variation," *Sol. Energy Mater. Sol. Cells*, vol. 173, pp. 96–105, 2017.

[2] M. A. Green *et al.*, "Solar cell efficiency tables (Version 53)," *Prog. Photovolt. Res. Appl.*, vol. 27, no. 1, pp. 3–12, 2019.

[3] F. Haase *et al.*, "Laser contact openings for local poly-Si-metal contacts enabling 26.1%-efficient POLO-IBC solar cells," *Sol. Energy Mater. Sol. Cells*, vol. 186, pp. 184–193, 2018.

[4] P. Padhamnath *et al.*, "Development of thin polysilicon layers for application in monoPoly$^{\mathrm{TM}}$ cells with screen-printed and fired metallization," *Sol. Energy Mater. Sol. Cells*, vol. 207, 2020, Art. no. 110358.

[5] H. E. Çiftpınar *et al.*, "Study of screen printed metallization for polysilicon based passivating contacts," *Energy Procedia*, vol. 124, pp. 851–861, 2017.

[6] N. Nandakumar *et al.*, "Approaching 23% with large-area monoPoly cells using screen-printed and fired rear passivating contacts fabricated by inline PECVD," *Prog. Photovolt. Res. Appl.*, vol. 15, no. 1, 2018, Art. no. 41.

[7] V. Arya *et al.*, "Laser ablation and Ni/Cu plating approach for tunnel oxide passivated contacts solar cells with variate polysilicon layer thickness: Gains and possibilities in comparison to screen printing," *Phys. Status Solidi A*, vol. 217, 2020, Art. no. 2000474.

[8] B. Grübel *et al.*, "Plated Ni/Cu/Ag for TOPCon solar cell metallization," in *Proc. 36th Eur. Photovolt. Sol. Energy Conf.*, 2019, pp. 1–5.

[9] S. Kluska *et al.*, "Plating for passivated-contact," *Photovolt. Int.*, vol. 44, pp. 98–110, 2020.

[10] L. Tous *et al.*, "22.4% bifacial n-PERT cells with Ni/Ag co-plated contacts and voc ∼691 mV," *Energy Procedia*, vol. 124, pp. 922–929, 2017.

[11] T. Hatt, J. Bartsch, S. Kluska, and M. Glatthaar, "Establishing the 'native oxide barrier layer for selective electroplated' metallization for bifacial silicon heterojunction solar cells," in *Proc. 15th Int. Conf. Concentrator Photovol. Syst.*, 2019, Art. no. 40005.

[12] A. Faes *et al.*, "Metallization and interconnection for high-efficiency bifacial silicon heterojunction solar cells and modules," *Photovolt. Int.*, vol. 41, pp. 65–76, 2018.

[13] K. Gensowski *et al.*, "Direct contact plating - Inline plating solution for ZEBRA IBC by local contacting," in *Proc. 8th Workshop Metallization Interconnection Crystalline Silicon Sol. Cells*, 2019, pp. 1–10.

[14] J. Bartsch *et al.*, "21.8% Efficient n-type solar cells with industrially feasible plated metallization," *Energy Procedia*, vol. 55, pp. 400–409, 2014.

[15] A. Mondon, M. N. Jawaid, J. Bartsch, M. Glatthaar, and S. W. Glunz, "Microstructure analysis of the interface situation and adhesion of thermally formed nickel silicide for plated nickel–copper contacts on silicon solar cells," *Sol. Energy Mater. Sol. Cells*, vol. 117, pp. 209–213, 2013.

[16] S. Roder *et al.*, "New approach for a combined process of an ultra-fast boron-oxygen defect regeneration and thermal contact treatment of Ni/Cu/Ag plated solar cells," in *Proc. 36th Eur. Photovolt. Sol. Energy Conf.*, 2019, pp. 457–463.

[17] A. Lennon, Y. Yao, and S. Wenham, "Evolution of metal plating for silicon solar cell metallisation," *Prog. Photovolt., Res. Appl.*, vol. 21, no. 7, pp. 1454–1468, 2013.

[18] V. Fakhfouri, D. Corinne, R. Julien, and S. A. Pasan, "Measurement accuracy and precision: The GridTOUCH contacting system," 2014. [Online]. Available: www.meyerburger.com

[19] D. K. Schroder, *Semiconductor Material and Device Characterization*. Hoboken, NJ, USA: IEEE Press, 2006.

[20] D. R. Lide, *CRC Handbook of Chemistry and Physics*, 86th ed. Boca Raton, FL, USA.: Taylor & Francis, 2004.

[21] H. Merhi, A. Fell, B. Grubel, M. Glatthaar, and S. Kluska, "Inhomogeneity of plated contacts for c-Si solar cells and their impact on solar cell efficiency," *IEEE J. Photovolt.*, vol. 10, no. 5, pp. 1455–1462, Sep. 2020.

[22] F. W. Peek, "The law of corona and the dielectric strength of air," *Proc. Amer. Inst. Electr. Eng.*, vol. 30, no. 7, pp. 1485–1561, 1911.

[23] Y. Yao, A. Lennon, B. S. Tjahjono, and S. R. Wenham, "Use of inductively-coupled-plasma measurements to monitor light-induced plating of silicon solar cells," *Sol. Energy Mater. Sol. Cells*, vol. 96, pp. 257–265, 2010.

[24] G. Gaspar *et al.*, "Influence of copper diffusion on lifetime degradation in n-type czochralski silicon for solar cells," *Energy Procedia* vol. 77, pp. 586–591, 2015.